ACS Photonics

Article

Cite This: ACS Photonics 2019, 6, 767−778

pubs.acs.org/journal/apchd5

Highly Efficient Deep Blue Aggregation-Induced Emission Organic Molecule: A Promising Multifunctional Electroluminescence Material for Blue/Green/Orange/Red/White OLEDs with Superior Efficiency and Low Roll-Off

Zeng Xu,[†] Jiabao Gu,[†] Xianfeng Qiao,[†] Anjun Qin,*[,†] Ben Zhong Tang,*[,†,‡] and Dongge Ma*[,†]

[†]Center for Aggregation-Induced Emission, Institute of Polymer Optoelectronic Materials and Devices, State Key Laboratory of Luminescent Materials and Devices, South China University of Technology, Guangzhou, 510640, China

[‡]Department of Chemistry, Hong Kong Branch of Chinese National Engineering Research Center for Tissue Restoration and Reconstruction, The Hong Kong University of Science & Technology, Clear Water Bay, Kowloon, Hong Kong, China

Supporting Information

ABSTRACT: For the constant demand of organic light-emitting diodes (OLEDs) with high efficiency, long lifetime, and low cost for display and lighting applications, the development of high-performance organic electroluminescence materials is key. Aggregation-induced emission (AIE) luminogens (AIEgens) provide a promising choice for their excellent performance in nondoped devices. Here we report a multifunctional deep blue AIE material, which can be used not only as an excellent blue emitter but also as a good host of green/orange/red phosphors. A deep blue nondoped OLED with a CIE_y of 0.08 and high external quantum efficiency (EQE) of 7.0% is achieved. Furthermore, a series of green/orange/red phosphorescent OLEDs with high efficiency and low roll-off are obtained. Impressively, hybrid white OLEDs (WOLEDs) based on the deep blue AIEgen exhibit simultaneously high CRI (>90), excellent efficiency (EQE_{max}> 25%, PE_{max} = 99.9 lm W^{-1} for two-color WOLEDs, PE_{max} = 60.7 lm W^{-1} for four-color WOLEDs), low roll-off ($PE_{1000nit}$ = 72.1 lm W^{-1} for two-color WOLEDs, $PE_{1000nit}$ = 43.5 lm W^{-1} for four-color WOLEDs), and superior stable color, indicative of the multifunction of AIEgens. Accordingly, this work opens a new direction for achieving high-performance OLEDs, particularly offering a smart but simple way to depress the efficiency roll-off and reduce the cost of OLEDs for practical applications.

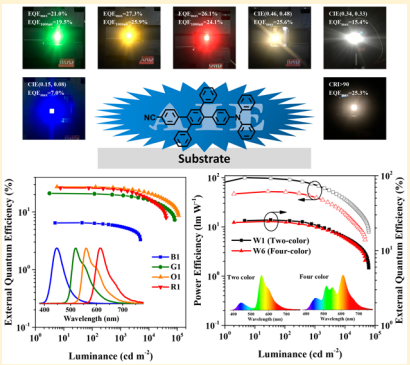

KEYWORDS: *deep blue, aggregation-induced emission, host, hybrid WOLEDs, superior efficiency, low roll-off*

The rapid development of organic light-emitting diodes (OLEDs) in lighting and panel display applications has an urgent demand for high-performance OLEDs with low efficiency roll-off and simple fabrication processes.[1] OLED emitters with different mechanisms have been constantly developed to satisfy the high requirement of their commercial applications. Currently, the conventional fluorophors and precious transition metal-based phosphors are first- and second-generation OLED emitters. Different from the conventional fluorophors, which harvest only singlet excitons (25% of all excitons), the phosphors are able to harvest 100% excitons to achieve high-performance OLEDs.[2] Yet, due to the rarity of the transition metal and the high price of transition metal-based phosphors, metal-free luminophores with the character of thermally activated delayed fluorescence (TADF) were developed.[3,4] The TADF emitters exhibit a small energy gap (ΔE_{st}) between the lowest excited singlet state (S_1) and the lowest excited triplet state (T_1), so that they can also achieve the ideal 100% internal quantum efficiency (IQE) by harvesting both singlet and triplet excitons via efficient reverse intersystem crossing (RISC). What is more, there are still another two mechanisms to employ triplet excitons for high-efficiency emission, which are hybridized local and charge-transfer (HLCT) state[5] and triplet−triplet annihilation (TTA),[6,7] which utilize the high-lying triplet excitons or the annihilation of two triplet excitons, respectively. However, most of the phosphors and TADF materials suffer from the aggregation-caused quenching (ACQ) problem to different extents and exhibit relatively low quantum yields in nondoped films. So, most of them, especially phosphors and TADF emitters, have to be dispersed in proper hosts with high triplet levels to alleviate the intrinsic ACQ process. Particularly, the phosphors and TADF emitters still face the severe problems of short lifetime of blue emitters and large efficiency roll-off at high luminance,[8,9] which largely restrict their applications. Although HLCT and TTA emitters are superior in nondoped devices and theoretically achieve respectively, 100% and 62.5% IQEs and low roll-off property,[5,10] their low T_1 makes them

Received: December 14, 2018
Published: February 12, 2019

DOI: 10.1021/acsphotonics.8b01724
ACS Photonics 2019, 6, 767−778

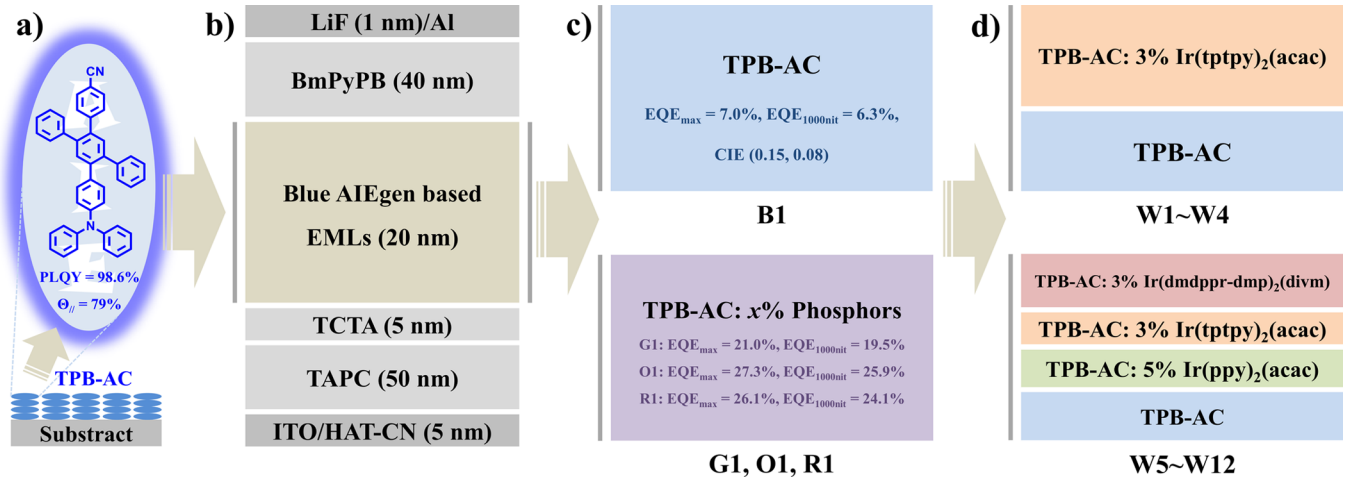

Figure 1. Schematic configurations of the developed monochromatic and white OLEDs based on multifunctional AIEgen TPB-AC. (a) Molecular structure of the selected deep blue AIEgen (TPB-AC) with a high quantum yield (QY) of 98.6% and a horizontal dipole ratio ($\Theta_{\parallel}$) of 79%. (b) Schematic configurations of AIEgen-based EMLs. (c) EML structures of monochromatic OLEDs (B1, G1, O1, R1) based on TPB-AC. (d) EML structures of two-color WOLEDs (W1−W4) and four-color WOLEDs (W5−W12) based on TPB-AC.

unable to act as a good luminescent host, and the exciton quenching problem has to be considered in the design of white OLEDs. From the perspective of comprehensive performance and application cost, the development of multifunctional high-performance OLED materials is still very urgent.

Aggregation-induced emission luminogens (AIEgens) are attractive alternatives because of the important characteristic of a strong emission of light in aggregate or solid states.[11,12] As we know, due to the highly twisted conformation and weak intermolecular interaction, AIEgens are able to efficiently suppress exciton annihilation in solid-state film. With this superior feature, AIEgens exhibit great potential as efficient pure emitters to fabricate nondoped OLEDs with high efficiency and low efficiency roll-off.[13−18] Such superiority will be extraordinarily prominent in AIEgens with deep blue emission. Some recent advances in material synthesis have fully demonstrated this possibility.[14,19,20] What is more, without complicated doping, OLEDs adopting AIEgens as emitters are more easily commercialized by simple processing technology and thus a low manufacturing cost. Therefore, how to develop such good AIEgens is particularly important for the fabrication of high-performance OLEDs.

In this work, we deeply investigate the electroluminescence (EL) properties of a bipolar deep blue AIEgen, namely, TPB-AC (4′-(4-(diphenylamino)phenyl)-5′-phenyl-[1,1′:2′,1″-ter-phenyl]-4- carbonitrile),[21] and the molecular structure of TPB-AC is shown in Figure 1a. It is found that TPB-AC is not only an excellent emitter to fabricate pure blue OLEDs with high efficiency and extremely low efficiency roll-off but also a very good host of phosphors to realize high efficiency, low roll-off red, and orange and green phosphorescent OLEDs, fully exhibiting its excellent multifunctionality. Thus, high-efficiency hybrid WOLEDs by simply using pure TPB-AC as a blue emitting layer and phosphors-doped TPB-AC as long-wavelength emitting layers are successfully fabricated, and they also exhibit extremely low efficiency roll-off at high luminance. It can be seen that the optimized deep blue nondoped OLEDs show impressive EL performances: (i) deep blue emission with Commission International de l'Eclairage (CIE) coordinates of (0.151, 0.080) at a luminance of 1000 cd m^{-2}; (ii) low turn-on voltage of 2.8 V, which is the lowest among deep blue AIE OLEDs with a CIE_y < 0.10; (iii) high efficiency and low roll-off; the maximum forward-viewing external quantum efficiency (EQE) reaches 7.0%, which is the highest of all deep-blue AIE OLEDs. Furthermore, the EQE can remain at 7.0% and 6.3% at the practical brightness of 100 and 1000 cd m^{-2}, respectively. The fabricated green/orange/red phosphorescent OLEDs using TPB-AC as host also exhibit excellent EL performances. The maximum EQEs arrive at 21.0% for green, 27.3% for orange, and 26.1% for red; even at the practical luminance of 1000 cd m^{-2}, their efficiencies remain at 19.5%, 25.9%, and 24.1%, respectively. For the resulting two-color hybrid warm WOLEDs, they also show high efficiency and low roll-off. The maximum forward-viewing EQE and power efficiency (PE) reach 25.6% and 99.9 lm W^{-1} and keep 22.1% and 72.1 lm W^{-1} at the luminance of 1000 cd m^{-2}, respectively. The obtained pure white hybrid WOLEDs show a stable spectral property. The maximum forward-viewing EQE and PE achieve 15.4% and 47.0 lm W^{-1}, respectively, higher than previous reports.[22] Moreover, the high efficiency and high color-rendering index (CRI) four-color hybrid WOLEDs achieve a maximum forward-viewing PE of 60.7 lm W^{-1} and EQE of 25.3%, and the efficiencies can reach 43.5 lm W^{-1} and 21.3% at the luminance of 1000 cd m^{-2}. Significantly, the four-color WOLEDs exhibit a high CRI above 90, and the maximum CRI can reach 95. To the best of our knowledge, this should be the best EL performance of hybrid WOLEDs with a high CRI above 90.[23−25]

RESULTS AND DISCUSSION

Basic Photophysical Properties of TPB-AC. The used TPB-AC in our study is a deep blue AIEgen with very high quantum yield, which was measured to be 98.6% in neat film. The optical properties of TPB-AC are characterized by absorption and photoluminescence (PL) spectra, as shown in Figure S1. The absorption peak is at 355 nm. The PL peaks at room temperature and 77 K are at 448 and 445 nm, respectively. This indicates that the singlet energy of TPB-AC is 2.77 eV. The phosphorescence spectrum at 77 K exhibits a peak of 501 nm, suggesting that the triplet energy of TPB-AC is 2.48 eV. Such a value of triplet energy is higher than that of long-wavelength phosphor iridium(III) bis(2-phenylpyridine)-

DOI: 10.1021/acsphotonics.8b01724
ACS Photonics 2019, 6, 767−778

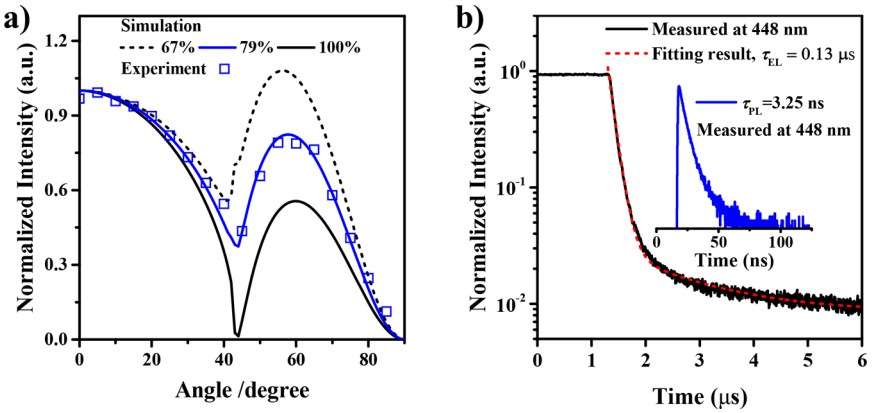

Figure 2. (a) Measured (symbols) p-polarized PL intensity (at PL peak wavelength) of a TPB-AC neat film as a function of the emission angles. (b) Transient electroluminescence spectra of a TPB-AC film. Inset: Transient photoluminescence spectra of a TPB-AC film.

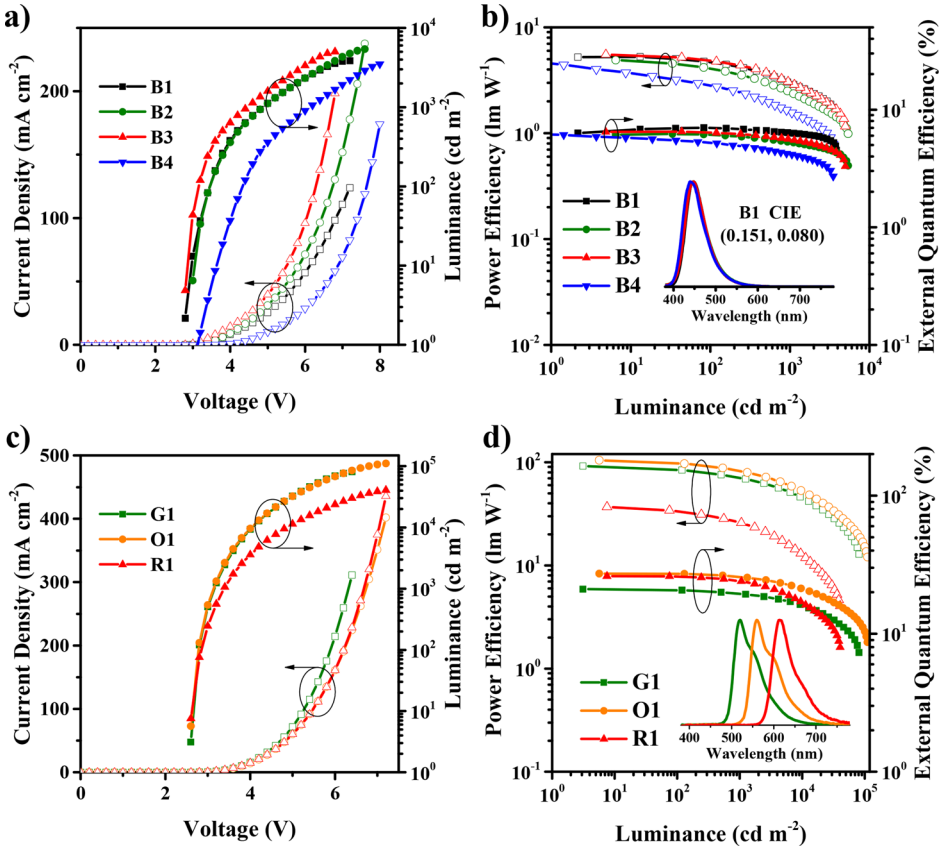

Figure 3. Electroluminescence characteristics of monochromatic OLEDs based on TPB-AC. (a) Current density−luminance−voltage characteristics of the resulting deep blue OLEDs with different ETLs. BmPyPB, TPBi, Bphen, and BCP as ETLs correspond to device B1, B2, B3, and B4, respectively. (b) Power and external quantum efficiencies as a function of luminance of the resulting deep blue OLEDs with different ETLs. Inset: EL spectra of device B1, B2, B3, and B4 at a luminance of 1000 cd m^{-2}. (c) Current density−luminance−voltage characteristics of the resulting devices G1, O1, and R1. (d) Power and external quantum efficiencies as a function of luminance of the resulting devices G1, O1, and R1. Inset: EL spectra of the resulting devices G1, O1, and R1 at a luminance of 1000 cd m^{-2}.

(acetylacetonate) ($Ir(ppy)_2(acac)$, 2.30 eV), iridium(III) bis(4-(4-*tert*-butylphenyl)thieno[3,2-*c*]pyridinato-N,$C^{2'}$)-acetylacetonate ($Ir(tptpy)_2(acac)$, 2.23 eV), and iridium(III) (2,8-dimethyl-4,6-nonanedionato-κO^4,κO^6)bis[2-[5-(2,6-dimethylphenyl)-3-(3,5-dimethylphenyl)-2-pyrazinyl-κN^1]-4,6-dimethylphenyl-κC] ($Ir(dmdppr\text{-}dmp)_2(divm)$, 2.00 eV), which are shown in Figure S3. As shown in Figure 2a, the TPB-AC neat film shows a high horizontal dipole ratio of 79%, and such a result indicates that TPB-AC may show a special mechanism in nondoped devices. Moreover, the lifetime of TPB-AC film in Figure 2b shows a short value of 3.25 ns recorded by transient PL spectrum. Moreover, the nondoped device based on TPB-AC (device B1) exhibits the character of one-phase exponential decay in a transient EL spectrum. These results indicate that TPB-AC harvests singlet excitons for the blue emission.

EL Performance of Monochromatic OLEDs. Based on the excellent photophysical properties of TPB-AC film, a

DOI: 10.1021/acsphotonics.8b01724
ACS Photonics 2019, 6, 767−778

Table 1. EL Performance of Devices B1, G1, O1, and R1

device	V_{on}[a] (V)	L_{max}[b] (cd m^{-2})	CE[c] (cd A^{-1})	PE[c] (lm W^{-1})	EQE[c] (%)	λ_{max}[d] (nm)	CIE[d] (x, y)
B1	2.8	3861.94	5.2/4.6	5.3/3.0	7.0/6.3	448	(0.15, 0.08)
G1	2.6	81 953.40	76.1/70.8	92.0/71.1	21.0/19.5	520	(0.33, 0.63)
O1	2.6	110 907.65	86.7/82.2	104.7/83.0	27.3/25.9	560	(0.49, 0.51)
R1	2.6	40 532.96	30.5/28.1	36.8/26.2	26.1/24.1	614	(0.66, 0.34)

[a]V_{on} is the turn-on voltage, which is measured at 1 cd m^{-2}. [b]L_{max} is the maximum luminance. [c]CE, PE, and EQE are the current efficiency, power efficiency, and external quantum efficiency, respectively. Order of measured value: maximum, then values at 1000 cd m^{-2}. [d]λ_{max} represents the peak wavelength of spectra. CIE is the Commission Internationale de l'Eclairage coordinates. λ_{max} and CIE are measured at 1000 cd m^{-2}.

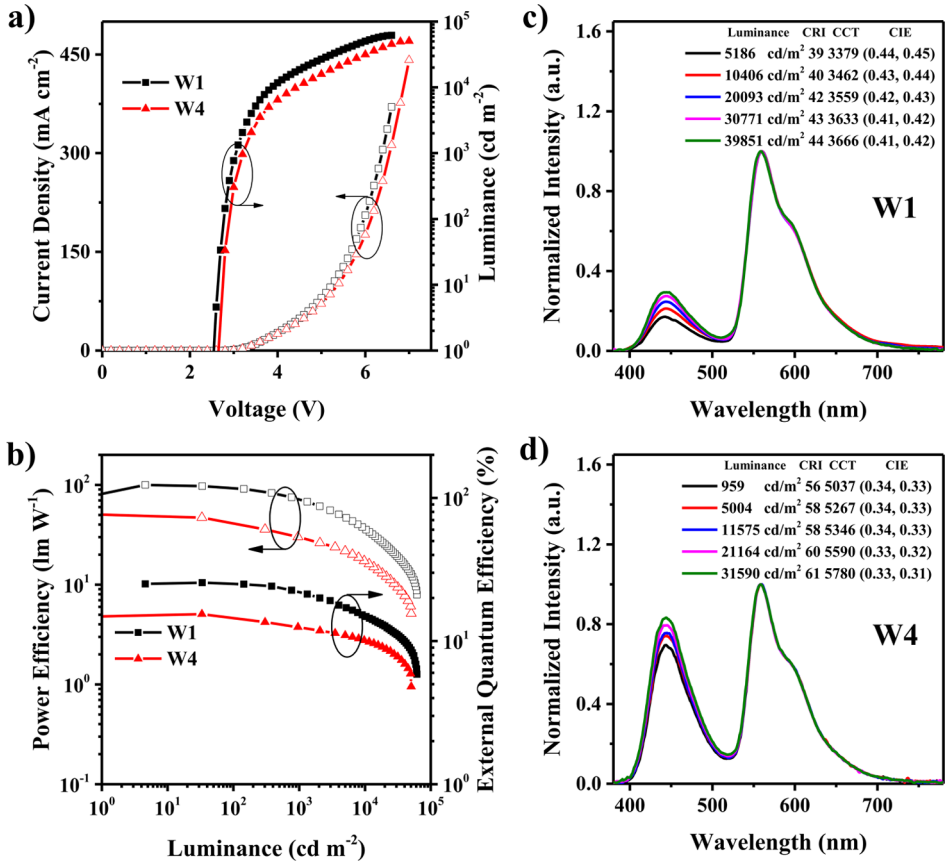

Figure 4. EL characteristics of two-color hybrid WOLEDs based on TPB-AC. (a) Current density−luminance−voltage characteristics of devices W1 and W4. (b) Power and external quantum efficiencies as a function of luminance for devices W1 and W4. (c) Normalized EL spectra of device W1 at different luminances. (d) Normalized EL spectra of device W4 at different luminances.

scheme of investigating multifunctionality of TPB-AC is provided in Figure 1. As shown in Figure 1b and c, the nondoped blue OLEDs using TPB-AC as emitter are manufactured with the structure (device B1, 2, 3, 4) of indium tin oxide (ITO)/1,4,5,8,9,11-hexaazatriphenylene hexacarbonitrile (HAT-CN, 5 nm)/1-bis[4-[*N*,*N*-di(4-tolyl)amino]-phenyl]cyclohexane (TAPC, 50 nm)/4,4′,4″-tri(*N*-carbazolyl)-triphenylamine (TCTA, 5 nm)/TPB-AC (20 nm)/ETLs (40 nm)/LiF (1 nm)/Al (120 nm), where ITO acts as the anode, TAPC and TCTA are used as the hole-transporting and electron/exciton-blocking layers, 1,3-bis[3,5-di(pyridin-3-yl)-phenyl]benzene (BmPyPB), 2,2′,2″-(1,3,5-benzinetriyl)tris(1-phenyl-1*H*-benzimidazole) (TPBi), 4,7-diphenyl-1,10-phenanthroline (Bphen), or 2,9-dimethyl-4,7-diphenyl-1,10-phenanthroline (BCP) is chosen for the electron-transporting layer (ETL), HAT-CN and LiF are selected for the hole- and electron-injecting layers, respectively, and Al acts as the cathode. In the fabricated blue devices, TPB-AC neat film is used as the emitting layer. Upon choosing different ETLs, we get four deep blue OLEDs with CIE$_{x,y}$(0.15, 0.08), and it can be seen that device B1 shows the best EL performance among these devices. Its turn-on voltage (1 cd m^{-2}) is as low as 2.8 V, and the maximum forward-viewing EQE and power efficiency reach 7.0% and 5.3 lm W^{-1} (Figure 3b and Table 1), respectively. In addition, at the luminance of 1000 cd m^{-2}, the forward-viewing EQE can also reach 6.3%, exhibiting a very low roll-off. Compared with the recent performance of deep blue OLEDs with CIE$_y$ < 0.10 (As shown in Table S3), OLEDs based on TPB-AC exhibit high efficiency and low roll-off simultaneously, which are better than most of the reported deep blue materials. As we see, the EQE of the fabricated blue OLEDs exceeds the limited efficiency of fluorescence emission by 5%.[26] In order to clarify the improvement mechanism, we studied the molecular orientation property of TPB-AC. The measured p-polarized PL intensity at 448 nm as a function of emission angle for TPB-AC film is shown in Figure 2a. The

DOI: 10.1021/acsphotonics.8b01724
ACS Photonics 2019, 6, 767−778

Table 2. Summary of EL Performances of the Resulting Hybrid WOLEDs

device	V_{on}[a] (V)	L_{max}[b] (cd m^{-2})	CE[c] (cd A^{-1})	PE[c] (lm W^{-1})	EQE[c] (%)	CRI[d]	CIE[e] (x, y)
W1	2.6	61 730.34	83.5/69.8	99.9/72.1	25.6/22.1	40	(0.46, 0.48)
W4	2.6	50 554.33	41.9/30.6	47.0/29.9	15.4/12.5	58	(0.34, 0.33)
W6	2.6	32 640.69	54.8/48.7	60.7/43.5	25.3/21.3	92	(0.48, 0.45)
W9	2.6	34 173.65	45.7/43.4	49.3/41.8	21.7/19.6	94	(0.47, 0.45)

[a]V_{on} is the turn-on voltage, which is measured at 1 cd m^{-2}. [b]L_{max} is the maximum luminance. [c]Order of measured value: maximum, then values at 1000 cd m^{-2}. [d]Color rendering index (CRI) is measured at 10 000 cd m^{-2}. [e]CIEs are measured at 1000 cd m^{-2}.

experimental curve is compared to the simulated curves of fully horizontal dipoles and isotropic dipoles to determine the horizontal dipole ratio $\Theta_{\parallel}$ of TPB-AC ($\Theta_{\parallel}$ = 100% for fully horizontal dipoles, $\Theta_{\parallel}$ = 67% for the isotropic dipoles). It can be seen that the $\Theta_{\parallel}$ of the TPB-AC molecule reaches 79% by classical dipole model fitting, indicating that the TPB-AC molecule is preferentially oriented along the horizontal direction. The $\Theta_{\parallel}$ of TPB-AC with an additional TCTA layer also achieves a value of as high as 77% (Figure S2a). Such highly oriented character should be greatly helpful to enhance the efficiency of TPB-AC-based blue OLEDs.

Furthermore, employing TPB-AC as host, we examine the EL performance of green/orange/red phosphorescent OLEDs with the structure of ITO/HAT-CN (5 nm)/TAPC (50 nm)/TCTA (5 nm)/TPB-AC: dopant (20 nm)/BmPyPB (40 nm)/LiF (1 nm)/Al (120 nm). For green device G1, 5 wt % Ir(ppy)$_2$(acac)-doped TPB-AC is used as the emitting layer, and its maximum forward-viewing current efficiency (CE), PE, and EQE reach 76.1 cd A^{-1}, 92.0 lm W^{-1}, and 21.0%, respectively (Figure 3d and Table 1). Moreover, device G1 shows a low EQE roll-off of 7.1% at a luminance of 1000 cd m^{-2}. For orange device O1, 3 wt % Ir(tptpy)$_2$(acac)-doped TPB-AC is used as the emitting layer. Impressively, device O1 shows the maximum forward-viewing CE, PE, and EQE of 86.7 cd A^{-1}, 104.7 lm W^{-1}, and 27.3%, respectively (Figure 3d and Table 1). Its maximum luminance exceeds 110 000 cd m^{-2}, and at the luminance of 1000 cd m^{-2}, the efficiency roll-off is as low as 5.1%. For red device R1, 3 wt % Ir(dmdppr-dmp)$_2$(divm)-doped TPB-AC is used as the emitting layer. A very good red emission with CIE coordinates of (0.66, 0.34) is obtained. It can be seen that device R1 achieves the maximum forward-viewing CE, PE, and EQE of 30.5 cd A^{-1}, 36.8 lm W^{-1}, and 26.1% (Figure 3d and Table 1), respectively, and also shows a low EQE roll-off of 7.7% at the luminance of 1000 cd m^{-2}. Encouragingly, all the fabricated devices G1, O1, and R1 exhibit high-efficiency and low-efficiency roll-off at high luminance, fully exhibiting the good performance of TPB-AC material as host in phosphorescence OLEDs from these advantages: (a) Due to the highly twisted structure of TPB-AC, the distribution of excitons becomes relatively uniform; eventually the Dexter energy transfer quenching process is greatly suppressed, which results in more triplet excitons to transfer from host to guest; (b) the bipolar characteristic of TPB-AC contributes to broadening the charge and exciton distribution,[27] which can greatly reduce the charge/exciton quenching process of triplet−triplet annihilation (TTA) and triplet-polaron quenching (TPQ); (c) the high horizontal dipole ratios of Ir(tptpy)$_2$acac- and Ir(dmdppr-dmp)$_2$(divm)-doped TPB-AC films (achieving 69% and 78%, respectively, as shown in Figure S2b) also enhance the out-coupling of light. Obviously, TPB-AC is not only a very good blue emission material itself but also an excellent phosphor host that is used to fabricate high-performance OLEDs.

EL Performance of Two-Color Hybrid WOLEDs. Due to the high performance of monochromatic devices based on TPB-AC, two schemes of two-color and four-color hybrid WOLEDs are presented in Figure 1d. We used a pure TPB-AC as the blue emitting layer near the HTL and a phosphor-doped TPB-AC host as the long-wavelength emitting layers near the ETL to construct the hybrid WOLEDs in order to achieve high-performance white emission. The detailed structure of the optimized two-color hybrid WOLED (device W1) is ITO/HATCN (5 nm)/TAPC (50 nm)/TCTA (5 nm)/TPB-AC (8 nm)/TPB-AC: 3 wt % Ir(tptpy)$_2$(acac) (12 nm)/BmPyPB (40 nm)/LiF (1 nm)/Al (120 nm). It can be seen that device W1 emits a maximum forward-viewing CE, PE, and EQE of 83.5 cd A^{-1}, 99.9 lm W^{-1}, and 25.6%, respectively (Figure 4b and Table 2), and also shows a rather low roll-off, in which the PE and EQE yet remain at 72.1 lm W^{-1} and 22.1% at the luminance of 1000 cd m^{-2}, respectively. Additionally, the white emission of device W1 is rather stable, where the CIE coordinates change slightly from (0.43, 0.44) to (0.41, 0.42) when the luminance goes from 5185.85 cd m^{-2} to 30 770.50 cd m^{-2}. Clearly, the blue emission of device W1 totally comes from the TPB-AC molecule and the orange emission from the doped Ir(tptpy)$_2$(acac), which is in accordance with device O1. For comparison, we further fabricated devices W2, W3, and W4 with the same configuration as device W1 except for the thickness of the blue EML (L_B) and the orange EML (L_O) (W2: L_B = 10 nm, L_O = 10 nm; W3: L_B = 12 nm, L_O = 8 nm; W4: L_B = 14 nm, L_O = 6 nm), and the performances of devices W2, W3, and W4 are shown in Figures 4 and S5 and Table S2. Consequently, the blue emission becomes higher with the increase of L_B and the simultaneous decrease of L_O (Figures 4c,d, S5c,d). Furthermore, as shown in Figure 4d, device W4 exhibits pure white emission with CIE coordinates of (0.34, 0.33) at the luminance of 1000 cd m^{-2}, which is approaching the white equivalent point of (0.33, 0.33). Also, device W4 shows a high forward-viewing PE and EQE of 47.0 lm W^{-1} and 15.4%, respectively, and fairly stable spectral profile with a small CIE coordinate variation of (0.01, 0.01) when the luminance goes from 958.51 cd m^{-2} to 21163.96 cd m^{-2}. In fact, both the warm-white device W1 and the pure-white device W4 show the highest efficiency in hybrid WOLEDs with similar white emission in the past reports (as shown in Table S4), suggesting that the TPB-AC molecule is an excellent blue emitter and host, thus efficiently harvesting 100% excitons by such a device structure.

EL Performance of Four-Color Hybrid WOLEDs. To enhance CRI, we fabricated four-color hybrid WOLEDs. The optimized device W6 has the structure ITO/HATCN (5 nm)/TAPC (50 nm)/TCTA (5 nm)/TPB-AC (8 nm)/TPB-AC: 5 wt % Ir(ppy)$_2$(acac) (3 nm)/TPB-AC: 3 wt % Ir(tptpy)$_2$(acac) (2 nm)/TPB-AC: 3 wt % Ir(dmdppr-dmp)$_2$(divm) (9 nm)/BmPyPB (40 nm)/LiF (1 nm)/Al (120 nm). As shown in Figure 5c, device W6 exhibits an

DOI: 10.1021/acsphotonics.8b01724
ACS Photonics 2019, 6, 767−778

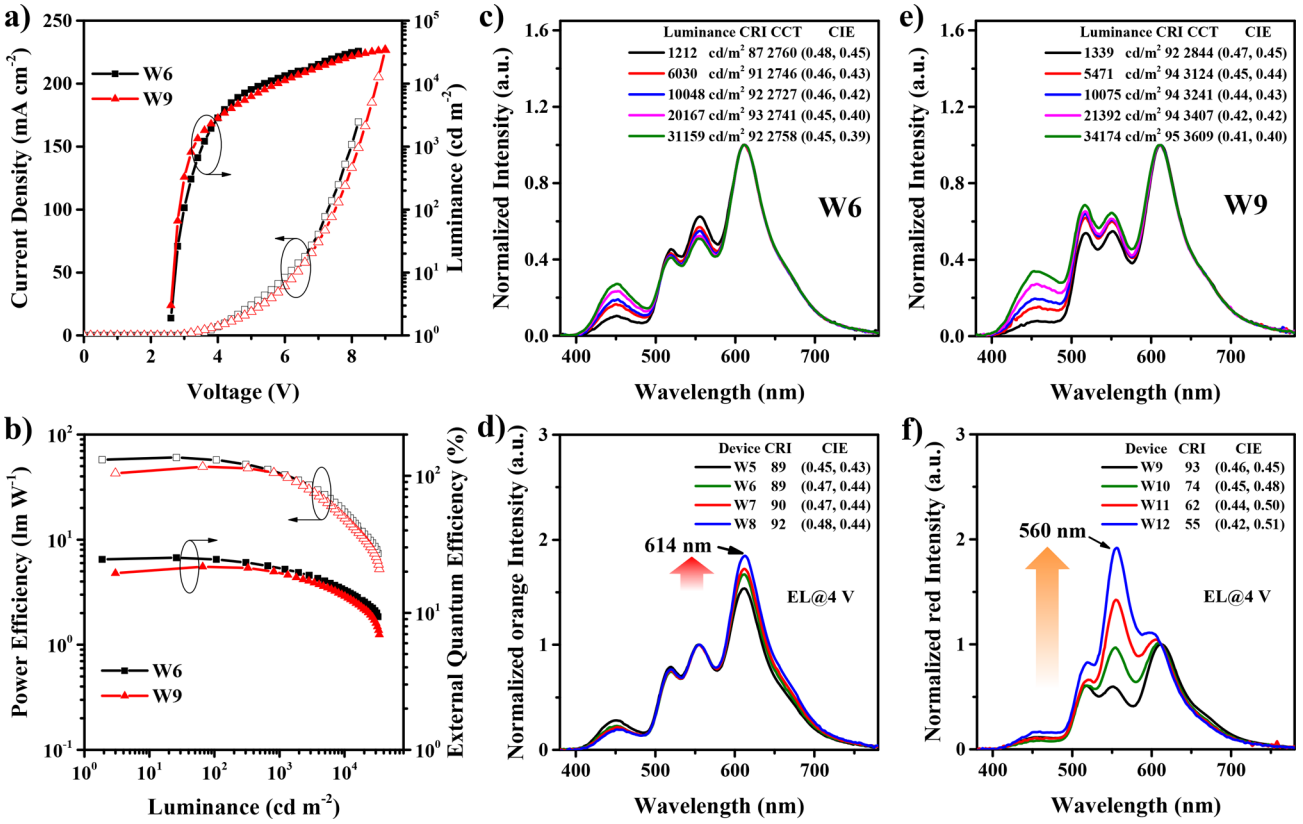

Figure 5. EL characteristics of four-color hybrid WOLEDs based on TPB-AC. (a) Current density−luminance−voltage characteristics of devices W6 and W9. (b) Power and external quantum efficiencies as a function of luminance for devices W6 and W9. (c) Normalized EL spectra of device W6 at different luminance. (d) EL spectra with normalized orange intensity of devices W5, W6, W7, and W8 at a voltage of 4 V, in which the relative intensity of red emission is increased (614 nm). (e) Normalized EL spectra of device W9 at different luminances. (f) EL spectra with normalized red intensity of devices W9, W10, W11, and W12 at a voltage of 4 V, in which the relative intensity of orange emission is increased (560 nm).

excellent EL performance with a high CRI above 90 when the luminance is higher than 4000 cd m^{-2}, and a low turn-on voltage of 2.6 V is achieved. Moreover, device W6 shows the maximum forward-viewing CE, PE, and EQE of 54.8 cd A^{-1}, 60.7 lm W^{-1}, and 25.3%, respectively, which remain at 48.7 cd A^{-1}, 43.5 lm W^{-1}, and 21.3% at the luminance of 1000 cd m^{-2}, respectively, showing a low roll-off. Moreover, to study the effect of red EML, three other WOLEDs of W5, W7, and W8 with the same configuration as device W6 except for the thickness of the red EMLs (8, 10, and 11 nm for W5, W7, and W8, respectively) are fabricated, and the device performances are shown in Figure S6 and Table S2. From Figure 5d, we can find that the intensity of relative red emission in devices W5, W6, W7, and W8 only grows slightly with the thickness increase, indicating that the exciton recombination zone in these devices is not in the red EML and the red emission should be the energy-transfer process. As we see, devices W5, W7, and W8 exhibit similar EL performance to device W6. The maximum forward-viewing PEs of 61.0, 56.2, and 52.2 lm W^{-1} and EQEs of 23.2, 24.7, and 24.5% are obtained, respectively. At a luminance of 1000 cd m^{-2}, the values of PEs reach 40.1, 40.9, and 40.2 lm W^{-1} and EQEs are 19.8, 20.8, and 20.7% for devices W5, W7, and W8, respectively. Their CRIs arrive at 92, 92, and 93 at the luminance of 5000 cd m^{-2}, respectively. To the best of our knowledge, combined with the summarized recent performances of WOLEDs with high CRIs in Table S5, this should be the best results of hybrid WOLEDs considering both high efficiency, low roll-off, and high CRI above 90. Because the orange phosphor $Ir(tptpy)_2(acac)$ doped in TPB-AC achieves a higher efficiency, we changed the thickness of the orange emission layer to get insight into the four-color WOLEDs. The device configurations are ITO/HATCN (5 nm)/TAPC (50 nm)/TCTA (5 nm)/TPB-AC (8 nm)/TPB-AC: 5 wt % $Ir(ppy)_2(acac)$ (3 nm)/TPB-AC: 3 wt % $Ir(tptpy)_2(acac)$ (L_O)/TPB-AC: 3 wt % $Ir(dmdppr\text{-}dmp)_2(divm)$ (7 nm)/BmPyPB (40 nm)/LiF (1 nm)/Al (120 nm), where devices W9, 10, 11, and 12 correspond to L_O = 1, 2, 3, and 4 nm, respectively, and their EL performances are shown in Figure S7 and Table S2. Device W9 shows a maximum forward-viewing CE, PE, and EQE of 45.7 cd A^{-1}, 49.3 lm W^{-1}, and 21.7%, which remain at 43.4 cd A^{-1}, 41.8 lm W^{-1}, and 19.6% at a luminance of 1000 cd m^{-2}, respectively. Impressively, device W13 shows a high CRI above 90 when the luminance goes from 326.99 cd m^{-2} to 34 173.65 cd m^{-2}, and a maximum CRI of 95 is achieved at a luminance of 34 173.65 cd m^{-2} with CIE coordinates of (0.41, 0.40). As shown in Figure 5f, both the orange emission intensity and device efficiencies grow with an increase in the $Ir(tptpy)_2(acac)$-doped layer thickness. As seen, device W10 shows a higher maximum CE, PE, and EQE of 59.7 cd A^{-1}, 65.6 lm W^{-1}, and 24.5%, respectively. Moreover, the efficiencies remain at 57.9 cd A^{-1}, 57.8 lm W^{-1}, and 22.5% at a luminance of 1000 cd m^{-2}, similarly displaying a very low efficiency roll-off. The spectra also are relatively stable, with a CRI of 73 at a luminance of 1000 cd m^{-2} (Figure S7c). However, as we see, although devices W11 and W12 could achieve higher

DOI: 10.1021/acsphotonics.8b01724
ACS Photonics 2019, 6, 767−778

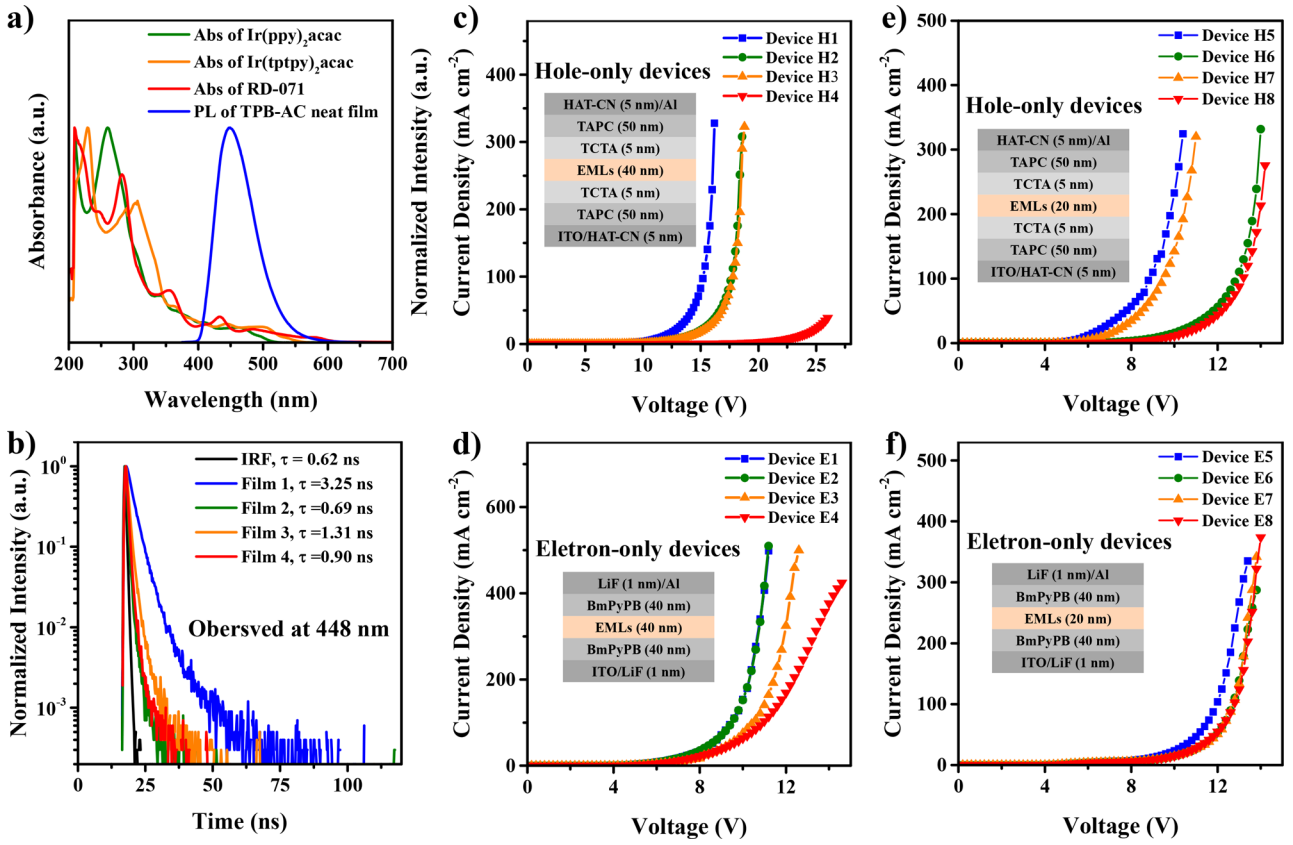

Figure 6. Energy-transfer and carrier-trapping process in AIE-WOLEDs. (a) Absorption spectra of $Ir(ppy)_2(acac)$, $Ir(tptpy)_2(acac)$, and $Ir(dmdppr\text{-}dmp)_2(divm)$ and PL spectrum of TPB-AC neat film. (b) Decay transients of TPB-AC in films 1−4. The structures of films 1−4 are TPB-AC (20 nm), TPB-AC: 5 wt % $Ir(ppy)_2(acac)$ (20 nm), TPB-AC: 3 wt % $Ir(tptpy)_2(acac)$ (20 nm), and TPB-AC: 3 wt % $Ir(dmdppr\text{-}dmp)_2(divm)$ (20 nm), respectively. (c) Current density−voltage characteristics of hole-only devices. Inset: Configurations of hole-only devices H1−H4. (d) Current density−voltage characteristics of electron-only devices. Inset: Configurations of electron-only devices E1−E4. EMLs are nondoped TPB-AC (H1, E1), TPB-AC: 5 wt % $Ir(ppy)_2(acac)$ (H2, E2), TPB-AC: 3 wt % $Ir(tptpy)_2(acac)$ (H3, E3), and TPB-AC: 3 wt % $Ir(dmdppr\text{-}dmp)_2(divm)$ (H4, E4). (e) Current density−voltage characteristics of hole-only devices. Inset: Configurations of hole-only devices H5−H8. (f) Current density−voltage characteristics of electron-only devices. Inset: Configurations of electron-only devices E5−E8. EMLs are TPB-AC for device H5 or E5, TPB-AC (8 nm)/TPB-AC: 3 wt % $Ir(tptpy)_2(acac)$ (12 nm) for device H6 or E6, TPB-AC (16 nm)/TPB-AC: 3 wt % $Ir(tptpy)_2(acac)$ (4 nm) for device H7 or E7, and TPB-AC (8 nm)/TPB-AC: 5 wt % $Ir(ppy)_2(acac)$ (3 nm)/TPB-AC: 3 wt % $Ir(tptpy)_2(acac)$ (2 nm)/TPB-AC: 3 wt % $Ir(dmdppr\text{-}dmp)_2(divm)$ (7 nm) for device H8 or E8, respectively.

efficiency, their emission deviates from the white light (Figure S7 and Table S2). This indicates that the thickness of the orange layer plays an important role in device efficiency and optical emission quality.

Origin of High EL Performance. It can be seen that the used AIEgen of TPB-AC as both blue emitter and host for long-wavelength phosphors is the key to our device structure design. Unlike conventional blue fluorescence emission materials with ACQ characters, TPB-AC can simultaneously achieve high efficiency and low roll-off due to its high quantum efficiency of a solid film in OLEDs without any doping.[9] What is more, the efficient energy transfer from TPB-AC to long-wavelength phosphors is also beneficial to the superior efficiency and low-efficiency roll-off, thus guaranteeing the design of highly efficient hybrid WOLEDs. In general, there are two basic strategies to construct multi-EML hybrid WOLEDs. One is inserting an interlayer between blue fluorophor and long-wavelength phosphor layers to prohibit the mutual exciton transfer and quenching processes[28,29] when the triplet level of the blue fluorophors is lower than that of the long-wavelength phosphors. However, such a strategy introduces additional interfaces, which may cause exciplex formation, and the voltage drop through the interlayers cannot be negligible, thus causing a reduction of power efficiency of the fabricated hybrid WOLEDs. Another is a noninterlayer strategy which requires the triplet level of the blue fluorophors to be higher than that of the long-wavelength phosphors,[30−32] and it is also expected that the used blue fluorophors can be as efficient a host of the long-wavelength phosphors in order to reduce the interface barrier and simplify the device processing. However, as we know, such fluorescent blue emission materials with high efficiency are very rare.[33] Fortunately, TPB-AC satisfies these requirements and solves the above problems; thus high-efficiency and low-efficiency roll-off hybrid WOLEDs can be well prepared by simple device structure and technology.

Generally there are two EL mechanisms in molecularly doped OLEDs: energy transfer and charge carrier trapping.[30,34] To get insight into the mechanisms of the resulting TPB-AC-based OLEDs, the absorption spectra of $Ir(ppy)_2(acac)$, $Ir(tptpy)_2(acac)$, and $Ir(dmdppr\text{-}dmp)_2(divm)$ and the PL spectrum of TPB-AC neat film are first measured. We can see from Figure 6a that they possess obvious spectral overlap, indicating that there exists an efficient energy transfer from TPB-AC to long-wavelength phosphors. Furthermore, the

DOI: 10.1021/acsphotonics.8b01724
ACS Photonics 2019, 6, 767−778

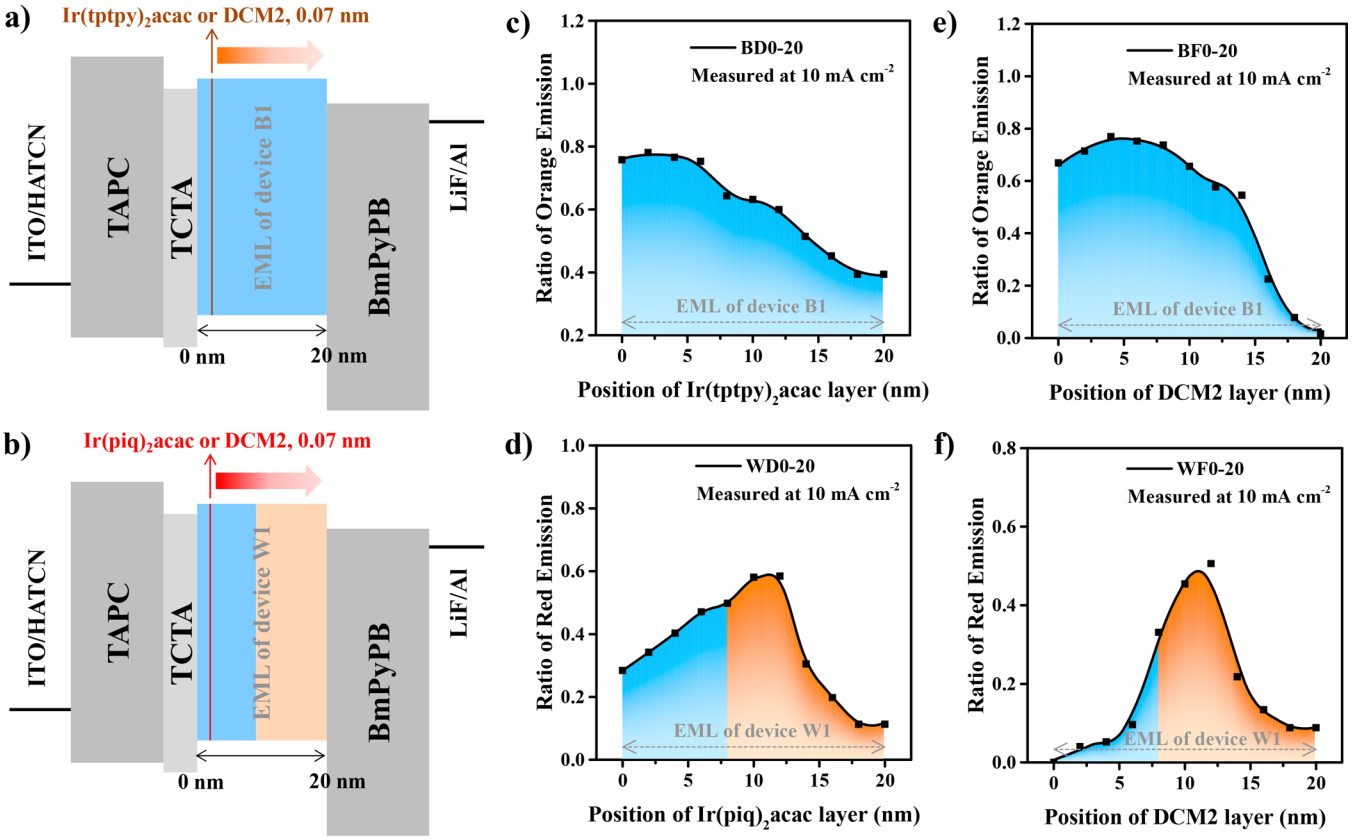

Figure 7. Device structure schemes that are used to determine the distribution of the exciton recombination zone in (a) devices BD0, 2, 4, 6, 8, 10, 12, 14, 16, 18, and 20, which use Ir(tptpy)$_2$(acac) as the inserted layer, device BF0, 2, 4, 6, 8, 10, 12, 14, 16, 18, and 20, which use DCM2 as the inserted layer, and (b) devices WD0, 2, 4, 6, 8, 10, 12, 14, 16, 18, and 20, which use Ir(tptpy)$_2$(acac) as the inserted layer, and devices WF0, 2, 4, 6, 8, 10, 12, 14, 16, 18, and 20, which use DCM2 as the inserted layer. The number represents the position of inserted long-wavelength phosphor or fluorophor. (c) Exciton distribution in device B1 using Ir(tptpy)$_2$(acac) as the inserted layer. (d) Exciton distribution in device W1 using Ir(tptpy)$_2$(acac) as the inserted layer. (e) Exciton distribution in device B1 using DCM2 as the inserted layer. (f) Exciton distribution in device W1 using DCM2 as the inserted layer.

transient PL decay properties of TPB-AC emission (recorded at 448 nm) in four organic films with different phosphor doping (TPB-AC for film 1, Ir(ppy)$_2$(acac)-doped TPB-AC for film 2, Ir(tptpy)$_2$(acac)-doped TPB-AC for film 3, and Ir(dmdppr-dmp)$_2$(divm)-doped TPB-AC for film 4) are studied. As shown in Figure S8, the structures of films 1−4 are TPB-AC (20 nm), TPB-AC: 5 wt % Ir(ppy)$_2$(acac) (20 nm), TPB-AC: 3 wt % Ir(tptpy)$_2$(acac) (20 nm), and TPB-AC: 3 wt % Ir(dmdppr-dmp)$_2$(divm) (20 nm), respectively. In Figure 6b, the lifetime of blue emission decreases from τ = 3.25 ns in film 1 to 0.69 ns in film 2, 1.31 ns in film 3, and 0.90 ns in film 4, further proving the efficient energy transfer from TPB-AC to long-wavelength phosphors. This also strongly indicates that the emission of green, orange, and red light in the resulting green, orange, and red OLEDs is due to the energy transfer from TPB-AC. Furthermore, we also fabricate hole-only and electron-only single-carrier devices with the structures of ITO/HAT-CN (5 nm)/TAPC (50 nm)/TCTA (5 nm)/EML/TCTA (5 nm)/TAPC (50 nm)/HAT-CN (5 nm)/Al (120 nm) and ITO/LiF (1 nm)/BmPyPB (40 nm)/EML (20 nm)/BmPyPB (40 nm)/LiF (1 nm)/Al (120 nm), respectively. Here, the EMLs are the same in hole-only or electron-only devices, where nondoped TPB-AC (40 nm) for device H1 or E1, TPB-AC: 5 wt % Ir(ppy)$_2$(acac) (40 nm) for device H2 or E2, TPB-AC: 3 wt % Ir(tptpy)$_2$(acac) (40 nm) for device H3 or E3, and TPB-AC: 3 wt % Ir(dmdppr-dmp)$_2$(divm) (40 nm) for device H4 or E4. The current density−voltage characteristics of these devices are shown in Figure 6c and d. We can see that the hole current is reduced for all phosphors and is more significant for red phosphor Ir(dmdppr-dmp)$_2$(divm). This means that green Ir(ppy)$_2$(acac) and orange Ir(tptpy)$_2$(acac) molecules have a certain trapping role in holes and the role is significant for the red Ir(dmdppr-dmp)$_2$(divm) molecule. Differently, the electron current is not changed for the green phosphor and is certainly reduced for orange and red phosphors, indicating that the green Ir(ppy)$_2$(acac) molecule does not have a trapping role in electrons and the orange and red phosphors trap electrons to a certain extent, but the trapping effect is obviously weaker than the hole trapping. All these processes indicate that the green emission is mainly due to energy transfer and the orange and red emissions also include a charge carrier trapping process besides energy transfer. As discussed below, because the exciton recombination zone in TPB-AC-based blue OLEDs is toward the HTL side, in order to minimize the hole-trapping effect of the doped phosphors as low as possible, we designed our WOLEDs with a blue/orange EML structure for two-color light and a blue/green/orange/red EML structure for four-color light, where the orange and red EMLs are far from the HTL spaced by blue and green layers. As shown in Figure 6e and f, hole-only and electron-only devices are fabricated by the EML structures of TPB-AC (20 nm) for device H5 or E5,

DOI: 10.1021/acsphotonics.8b01724
ACS Photonics 2019, 6, 767−778

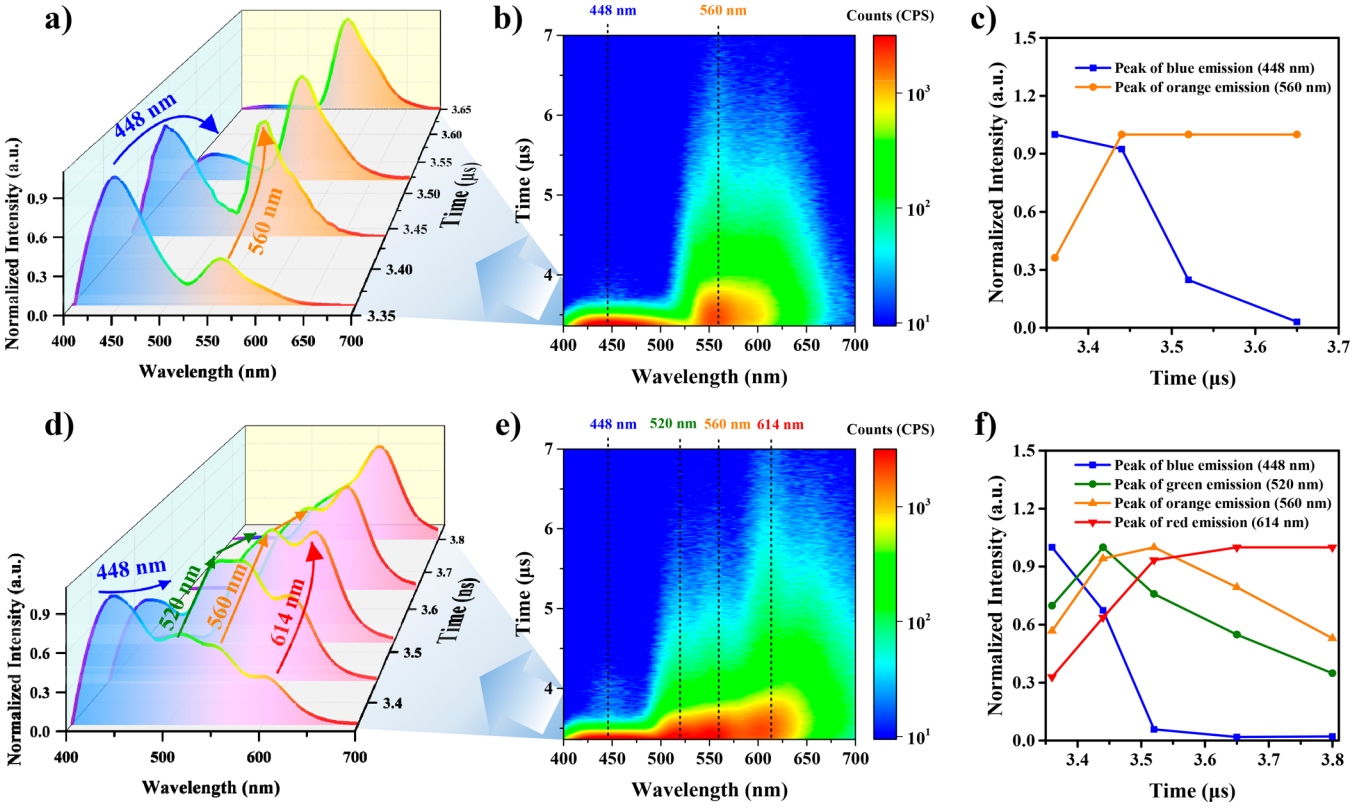

Figure 8. Energy-transfer processes revealed by time-resolved spectra in device W1 (a–c) and device W6 (d–f). (a) Normalized spectra of device W1 at different decay times. (b) Time-resolved spectra of device W1 at a current density of 10 mA cm^{-2}. (c) Blue and orange peak intensity of normalized spectra at different decay times for device W1. (d) Normalized spectra of device W6 at different decay times. (e) Time-resolved spectrum of device W6 at a current density of 10 mA cm^{-2}. (f) Blue, green, orange, and red peak intensity of normalized spectra at different decay times for device W6.

TPB-AC (8 nm)/TPB-AC: 3 wt % $Ir(tptpy)_2(acac)$ (12 nm) for device H6 or E6, TPB-AC (16 nm)/TPB-AC: 3 wt % $Ir(tptpy)_2(acac)$ (4 nm) for device H7 or E7, and TPB-AC (8 nm)/TPB-AC: 5 wt % $Ir(ppy)_2(acac)$ (3 nm)/TPB-AC: 3 wt % $Ir(tptpy)_2(acac)$ (2 nm)/TPB-AC: 3 wt % $Ir(dmdppr\text{-}dmp)_2(divm)$ (7 nm) for device H8 or E8. We can see that the electron current in devices E5–E8 is not changed by such sequential EMLs even though there is certain electron-trapping effect of orange and red phosphors, whereas the hole current is indeed reduced due to the hole-trapping role of orange and red phosphors, but the hole trapping can be greatly reduced by increasing the thickness of the blue TPB-AC layer (device H7). As we see below, the hole trapping of orange and red phosphors does not exist by the control of the exciton recombination zone in our hybrid WOLEDs. Therefore, it is concluded that the emission of green, orange, and red light in the fabricated hybrid WOLEDs is mainly due to energy transfer.

In order to more clearly clarify the recombination processes of excitons in our devices, we determined the exciton recombination region in both devices B1 and W1 by inserting an ultrathin long-wavelength phosphor or fluorophor into the EMLs, and the portion of photons coming from the inserted wavelength phosphor is selected to represent the exciton concentration. The device structure schemes are shown in Figure 7a and b. For device B1, we inserted an $Ir(tptpy)_2(acac)$ or DCM2 thin layer with a thickness of 0.07 nm every 2 nm across the 20 nm TPB-AC layer (the interface of TCTA and TPB-AC was set as 0 nm), and the measured spectra of devices BD0–20 at 10 mA cm^{-2} are shown in Figures S11 and S13. For device W1, the inserted thin layer is replaced by $Ir(piq)_2(acac)$ or DCM2 for the same operation, and the measured spectra of devices WD0–20 at 10 mA cm^{-2} are shown in Figures S12 and S14. To confirm the portions of inserted phosphor photons (η), a mathematical model is set up (Figure S10). As shown in Figure S10a, the normalized EL spectra of TPB-AC, $Ir(tptpy)_2(acac)$, $Ir(piq)_2(acac)$, and DCM2 are selected for the determination of η. For devices BD0–20 and BF0–20, η_O or η_R are easy to calculate through the intensity of blue and orange emission. However, for devices WD0–20 and WF0–20, the situation is complicated by the overlap of orange and red emission. Based on the model of $Ir(tptpy)_2(acac)$ and $Ir(piq)_2(acac)$ or DCM2 complex spectra in Figure S10b and c, we get the equation between η_R and the spectra of devices WD0–20. The values of η_O and η_R are given in Figures S11, 12, 13, and 14a–k. From the above results, we get the exciton distribution of devices B1 and W1. As shown in Figure 7c, d, e, and f, the excitons in devices B1 and W1 are mainly distributed in the TPB-AC layer that undertakes the large density of excitons, which supports the fact that the blue emission comes from the TPB-AC neat film in device W1. Such results also suggest the design requirement of the configuration of setting the $Ir(dmdppr\text{-}dmp)_2(divm)$-doped layer adjacent to the BmPyPB ETL in our four-color WOLEDs, thus reducing the charge carrier trapping on $Ir(dmdppr\text{-}dmp)_2(divm)$.

The energy transfer processes in two-color and four-color WOLEDs can be further proven through time-solved spectra.

DOI: 10.1021/acsphotonics.8b01724
ACS Photonics 2019, 6, 767–778

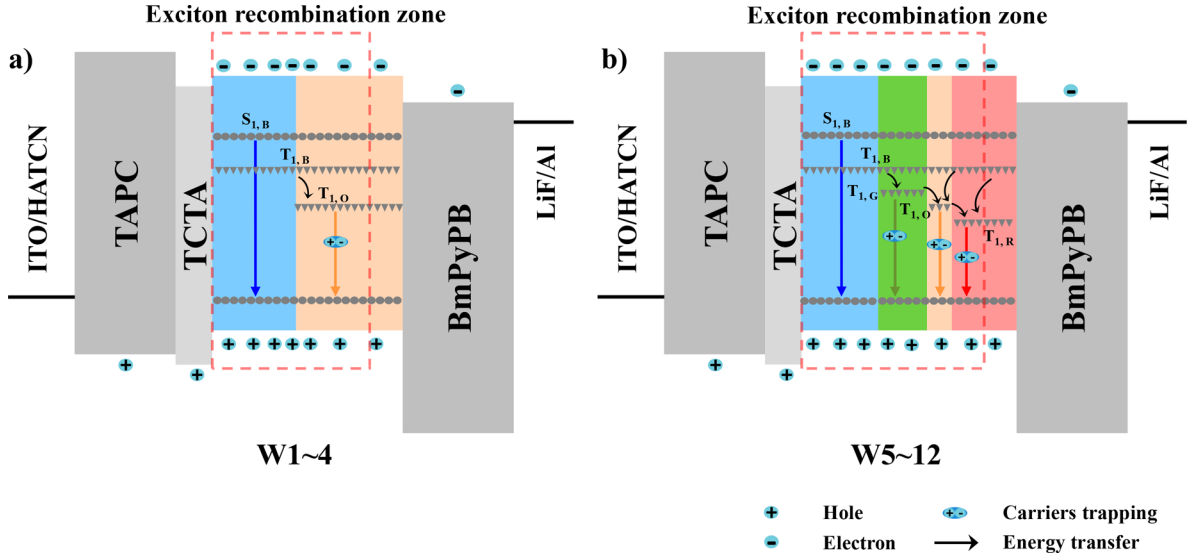

Figure 9. Working mechanism diagrams of the resulting hybrid WOLEDs. (a) Working mechanisms of two-color devices and (b) four-color devices.

As shown in Figure 8b, device W1 shows different behaviors of PL decay at 448 and 560 nm, which exhibit the features of fluorescence and phosphorescence, respectively. Moreover, as shown in Figure 8e, similar to W1, device W6 shows a quick PL decay at 448 nm and short PL decays at 520, 560, and 614 nm, which completely correspond to the emission features of TPB-AC, $Ir(ppy)_2(acac)$, $Ir(tptpy)_2(acac)$, and $Ir(dmdppr\text{-}dmp)_2(divm)$, respectively. From Figure 8a and c, we can see that the normalized orange light intensity is much lower than the blue emission in device W1 at the time of power off (t = 3.36 μs); after that, the normalized blue emission decreases rapidly, and the normalized orange emission increases as time progresses. From Figure 8d and f, we can see that the normalized green/orange/red light intensity is much lower than the blue emission in device W6 at the time of power off (t = 3.36 μs), and then, the normalized blue emission decreases rapidly. Moreover, the normalized green emission increases from 3.36 to 3.42 μs and then decreases from 3.42 μs. The normalized orange emission increases from 3.36 to 3.53 μs and then decreases. However, the normalized red emission grows with time from the point of 3.36 μs. Furthermore, transient PL spectra of films 2−4 are obtained in Figure S9, and lifetimes of green, orange, and red emission in films 2−4 are 1151, 1104, and 1072 ns, respectively. However, their lifetimes become different in EL, in which red emission has the longest lifetime, and then orange and green emissions show shorter lifetimes. Such results prove that green emission is quenched by orange or red phosphors, and orange emission is quenched by red phosphor. Clearly, the orange emission in device W1 and the green/orange/red emission in device W6 are directly observed at the time of power off (t = 3.36 μs), also supporting the fact of partial charge carrier trapping on green/orange/red phosphors, but the charge carrier trapping is not a main process.

2.6. Working Mechanisms. Based on the results of Figures 6, 7, and 8, the working mechanism diagrams of the TPB-AC-based two-color and four-color hybrid WOLEDs are shown in Figure 9a and b, respectively. For devices W1−4, the blue emission completely comes from the singlet excitons in the nondoped TPB-AC layer, whereas the orange emission then comes from the energy transfer of the triplet excitons in the nondoped TPB-AC layer to $Ir(tptpy)_2(acac)$ molecules as well as the triplet excitons formed directly on $Ir(tptpy)_2(acac)$ molecules by partial charge carrier trapping. For devices W5−12, similar to devices W1−4, the blue emission fully comes from the nondoped TPB-AC layer, and the green/orange/red emissions are due to the energy transfer from TPB-AC molecules. Moreover, the energy transfer from blue to green, to orange, and then to red also exists. Because the thickness of the green and orange layers are below the diffusion radius of triplet excitons, the energy transfer from a nondoped blue layer to orange/red or from green to red cannot be avoided.

CONCLUSIONS

AIEgen TPB-AC molecule shows a great potential in development of high-performance OLEDs due to their excellent multifunctionality, not only as a highly efficient blue emitter for high-efficiency blue OLEDs but also as a very good host for high-efficiency green/orange/red phosphorescence OLEDs and hybrid WOLEDs. More importantly, different from the organic emitters with an ACQ feature, AIE-based monochromatic and white OLEDs achieve excellent EL performance of superiority efficiency and low roll-off in a simple way, providing a new way for constructing high-performance OLEDs. It is predicted that AIE organic EL materials exhibit an extraordinary potential for next-generation OLEDs, which will greatly reduce the cost in commercial applications and open a new direction for the research of OLED materials and devices.

EXPERIMENTAL SECTION

Device Fabrication and Characterization. The AIE-based OLEDs were fabricated on clean glass substrates prepatterned with 180 nm of ITO with a sheet resistance of 10 Ω per square. The ITO surface was thoroughly cleaned in an ultrasonic detergent bath for 90 min, sequentially soaked in ultrasonic deionized water for 30 min (divided into 3 times, 10 min for each time), then dried at 120 °C for 1 h to remove the residual water. Afterward, the ITO substrates were treated with UV/ozone for 15 min before vacuum deposition. The pressure

DOI: 10.1021/acsphotonics.8b01724
ACS Photonics 2019, 6, 767−778

of the vacuum chamber was below 5×10^{-4} Pa. Then, the organic layers were deposited onto the substrates at the rate of 0.1−0.2 nm s^{-1}. Onto the organic layer, a LiF layer with a thickness of 1 nm was deposited at a rate of 0.02 nm s^{-1} to act as an electron injection layer. Finally, an Al layer with a thickness of 120 nm was deposited onto LiF at a rate of 0.6 nm s^{-1} to act as a cathode. The emission area of the devices was 4×4 mm^2 as shaped by the cross region of the anode and cathode. The EL spectra were taken by an optical analyzer, FlAME-S-VIS-NIR. Current density and luminance versus driving voltage characteristics were measured by a Keithley 2400 and a luminance meter LS-110, respectively. The external quantum efficiencies were calculated by assuming that the devices were Lambertian light sources. The time-resolved spectra of devices were measured by an Edinburgh Instruments F980 spectrometer. All the device measurements were carried out at room temperature under ambient laboratory conditions.

Measurement of Dipole Orientation of Nondoped TPB-AC Film. The dipole orientation of nondoped TPB-AC film was determined by angle-resolved and polarization-resolved PL.[35] A nondoped TPB-AC film with a thickness of 30 nm was deposited onto the substrate. Then the substrate was stuck to a half quartz cylinder prism by glue that has the same index as the cylinder. A continuous-wave He:Cd laser (325 nm) with a fixed angle of 45° to the substrate was employed as excitation source. p-Polarized emitted light was detected at the peak wavelength of the PL spectrum of nondoped TPB-AC film (448 nm).

Measurement of PL Quantum Yield. A 60 nm thickness TPB-AC film was grown on quartz substrates (1 cm × 1 cm) by vacuum deposition under a pressure of 5×10^{-4} Pa. Under an excitation wavelength of 355 nm, the PLQY of the TPB-AC neat film was measured to be 98.6% by an integrating sphere (Hamamatsu Absolute PL quantum yield spectrometer C11347).

■ ASSOCIATED CONTENT

Supporting Information

The Supporting Information is available free of charge on the ACS Publications website at DOI: 10.1021/acsphotonics.8b01724.

Additional information (PDF)

■ AUTHOR INFORMATION

Corresponding Authors

*E-mail: msdgma@scut.edu.cn.
*E-mail: msqinaj@scut.edu.cn.
*E-mail: tangbenz@ust.hk.

ORCID

Zeng Xu: 0000-0001-7552-8836
Xianfeng Qiao: 0000-0001-8633-8771
Anjun Qin: 0000-0001-7158-1808
Ben Zhong Tang: 0000-0002-0293-964X

Notes

The authors declare no competing financial interest.

■ ACKNOWLEDGMENTS

This work was supported by the National Natural Science Foundation of China (Grant Nos. 21788102, 51333007, 91433201, 11661131001) and Guangzhou Science & Technology Plan Project (201707020040). Particularly, we thank Prof. Chung-Chih Wu for providing help with the measurement of horizontal dipole ratios.

■ REFERENCES

(1) Song, J.; Kim, K. H.; Kim, E.; Moon, C. K.; Kim, Y. H.; Kim, J. J.; Yoo, S. Lensfree OLEDs with over 50% external quantum efficiency via external scattering and horizontally oriented emitters. *Nat. Commun.* **2018**, *9* (1), 3207.

(2) Baldo, M. A.; O'Brien, D. F.; You, Y.; Shoustikov, A.; Sibley, S.; Thompson, M. E.; Forrest, S. R. Highly efficient phosphorescent emission from organic electroluminescent devices. *Nature* **1998**, *395*, 151−154.

(3) Uoyama, H.; Goushi, K.; Shizu, K.; Nomura, H.; Adachi, C. Highly efficient organic light-emitting diodes from delayed fluorescence. *Nature* **2012**, *492* (7428), 234−8.

(4) Lee, J.; Chen, H. F.; Batagoda, T.; Coburn, C.; Djurovich, P. I.; Thompson, M. E.; Forrest, S. R. Deep blue phosphorescent organic light-emitting diodes with very high brightness and efficiency. *Nat. Mater.* **2016**, *15* (1), 92−98.

(5) Li, W.; Pan, Y.; Xiao, R.; Peng, Q.; Zhang, S.; Ma, D.; Li, F.; Shen, F.; Wang, Y.; Yang, B.; Ma, Y. Employing ~ 100% Excitons in OLEDs by Utilizing a Fluorescent Molecule with Hybridized Local and Charge-Transfer Excited State. *Adv. Funct. Mater.* **2014**, *24* (11), 1609−1614.

(6) Tang, X.; Bai, Q.; Shan, T.; Li, J.; Gao, Y.; Liu, F.; Liu, H.; Peng, Q.; Yang, B.; Li, F.; Lu, P. Efficient Nondoped Blue Fluorescent Organic Light-Emitting Diodes (OLEDs) with a High External Quantum Efficiency of 9.4% @ 1000 cd m^{-2} Based on Phenanthroimidazole−Anthracene Derivative. *Adv. Funct. Mater.* **2018**, *28* (11), 1705813.

(7) Chiang, C.-J.; Kimyonok, A.; Etherington, M. K.; Griffiths, G. C.; Jankus, V.; Turksoy, F.; Monkman, A. P. Ultrahigh Efficiency Fluorescent Single and Bi-Layer Organic Light Emitting Diodes: The Key Role of Triplet Fusion. *Adv. Funct. Mater.* **2013**, *23* (6), 739−746.

(8) Kuo, H. H.; Chen, Y. T.; Devereux, L. R.; Wu, C. C.; Fox, M. A.; Kuei, C. Y.; Chi, Y.; Lee, G. H. Bis-Tridentate Ir(III) Metal Phosphors for Efficient Deep-Blue Organic Light-Emitting Diodes. *Adv. Mater.* **2017**, *29* (33), 1702464.

(9) Chan, C.-Y.; Cui, L.-S.; Kim, J. U.; Nakanotani, H.; Adachi, C. Rational Molecular Design for Deep-Blue Thermally Activated Delayed Fluorescence Emitters. *Adv. Funct. Mater.* **2018**, *28* (11), 1706023.

(10) Kondakov, D. Y.; Pawlik, T. D.; Hatwar, T. K.; Spindler, J. P. Triplet annihilation exceeding spin statistical limit in highly efficient fluorescent organic light-emitting diodes. *J. Appl. Phys.* **2009**, *106* (12), 124510.

(11) Mei, J.; Hong, Y.; Lam, J. W.; Qin, A.; Tang, Y.; Tang, B. Z. Aggregation-induced emission: the whole is more brilliant than the parts. *Adv. Mater.* **2014**, *26* (31), 5429−5479.

(12) Mei, J.; Leung, N. L.; Kwok, R. T.; Lam, J. W.; Tang, B. Z. Aggregation-Induced Emission: Together We Shine, United We Soar! *Chem. Rev.* **2015**, *115* (21), 11718−940.

(13) Luo, J.; Xie, Z.; Lam, J. W. Y.; Cheng, L.; Tang, B. Z.; Chen, H.; Qiu, C.; Kwok, H. S.; Zhan, X.; Liu, Y.; Zhu, D. Aggregation-induced emission of 1-methyl-1,2,3,4,5-pentaphenylsilole. *Chem. Commun.* **2001**, No. 18, 1740−1741.

(14) Zhan, X.; Wu, Z.; Lin, Y.; Xie, Y.; Peng, Q.; Li, Q.; Ma, D.; Li, Z. Benzene-cored AIEgens for deep-blue OLEDs: high performance without hole-transporting layers, and unexpected excellent host for orange emission as a side-effect. *Chem. Sci.* **2016**, *7* (7), 4355−4363.

(15) Lin, G.; Chen, L.; Peng, H.; Chen, S.; Zhuang, Z.; Li, Y.; Wang, B.; Zhao, Z.; Tang, B. Z. 3,4-Donor- and 2,5-acceptor-functionalized dipolar siloles: synthesis, structure, photoluminescence and electroluminescence. *J. Mater. Chem. C* **2017**, *5* (20), 4867−4874.

(16) Qin, W.; Yang, Z.; Jiang, Y.; Lam, J. W. Y.; Liang, G.; Kwok, H. S.; Tang, B. Z. Construction of Efficient Deep Blue Aggregation-Induced Emission Luminogen from Triphenylethene for Nondoped

DOI: 10.1021/acsphotonics.8b01724
ACS Photonics 2019, 6, 767−778

Organic Light-Emitting Diodes. *Chem. Mater.* **2015**, *27* (11), 3892−3901.
(17) Liu, T.; Zhu, L.; Zhong, C.; Xie, G.; Gong, S.; Fang, J.; Ma, D.; Yang, C. Naphthothiadiazole-Based Near-Infrared Emitter with a Photoluminescence Quantum Yield of 60% in Neat Film and External Quantum Efficiencies of up to 3.9% in Nondoped OLEDs. *Adv. Funct. Mater.* **2017**, *27* (12), 1606384.
(18) Song, F.; Xu, Z.; Zhang, Q.; Zhao, Z.; Zhang, H.; Zhao, W.; Qiu, Z.; Qi, C.; Zhang, H.; Sung, H. H. Y.; Williams, I. D.; Lam, J. W. Y.; Zhao, Z.; Qin, A.; Ma, D.; Tang, B. Z. Highly Efficient Circularly Polarized Electroluminescence from Aggregation-Induced Emission Luminogens with Amplified Chirality and Delayed Fluorescence. *Adv. Funct. Mater.* **2018**, *28* (17), 1800051.
(19) Chen, B.; Liu, B.; Zeng, J.; Nie, H.; Xiong, Y.; Zou, J.; Ning, H.; Wang, Z.; Zhao, Z.; Tang, B. Z. Efficient Bipolar Blue AIEgens for High-Performance Nondoped Blue OLEDs and Hybrid White OLEDs. *Adv. Funct. Mater.* **2018**, *28*, 1803369.
(20) Liu, H.; Zeng, J.; Guo, J.; Nie, H.; Zhao, Z.; Tang, B. Z. High-Performance Non-doped OLEDs with Nearly 100% Exciton Use and Negligible Efficiency Roll-Off. *Angew. Chem., Int. Ed.* **2018**, *57* (30), 9290−9294.
(21) Li, L.; Nie, H.; Chen, M.; Sun, J.; Qin, A.; Tang, B. Z. Aggregation-enhanced emission active tetraphenylbenzene-cored efficient blue light emitter. *Faraday Discuss.* **2017**, *196*, 245−253.
(22) Liu, B.; Nie, H.; Zhou, X.; Hu, S.; Luo, D.; Gao, D.; Zou, J.; Xu, M.; Wang, L.; Zhao, Z.; Qin, A.; Peng, J.; Ning, H.; Cao, Y.; Tang, B. Z. Manipulation of Charge and Exciton Distribution Based on Blue Aggregation-Induced Emission Fluorophors: A Novel Concept to Achieve High-Performance Hybrid White Organic Light-Emitting Diodes. *Adv. Funct. Mater.* **2016**, *26* (5), 776−783.
(23) Liang, J.; Li, C.; Zhuang, X.; Ye, K.; Liu, Y.; Wang, Y. Novel Blue Bipolar Thermally Activated Delayed Fluorescence Material as Host Emitter for High-Efficiency Hybrid Warm-White OLEDs with Stable High Color-Rendering Index. *Adv. Funct. Mater.* **2018**, *28* (17), 1707002.
(24) Miao, Y.; Wang, K.; Zhao, B.; Gao, L.; Tao, P.; Liu, X.; Hao, Y.; Wang, H.; Xu, B.; Zhu, F. High-efficiency/CRI/color stability warm white organic light-emitting diodes by incorporating ultrathin phosphorescence layers in a blue fluorescence layer. *Nanophotonics* **2018**, *7* (1), 295−304.
(25) Zhang, D.; Duan, L.; Zhang, Y.; Cai, M.; Zhang, D.; Qiu, Y. Highly efficient hybrid warm white organic light-emitting diodes using a blue thermally activated delayed fluorescence emitter: exploiting the external heavy-atom effect. *Light: Sci. Appl.* **2015**, *4* (1), e232.
(26) Kido, J.; Iizumi, Y. Fabrication of highly efficient organic electroluminescent devices. *Appl. Phys. Lett.* **1998**, *73* (19), 2721−2723.
(27) Huang, J.; Nie, H.; Zeng, J.; Zhuang, Z.; Gan, S.; Cai, Y.; Guo, J.; Su, S.-J.; Zhao, Z.; Tang, B. Z. Highly Efficient Nondoped OLEDs with Negligible Efficiency Roll-Off Fabricated from Aggregation-Induced Delayed Fluorescence Luminogens. *Angew. Chem., Int. Ed.* **2017**, *56* (42), 12971−12976.
(28) Sun, Y.; Giebink, N. C.; Kanno, H.; Ma, B.; Thompson, M. E.; Forrest, S. R. Management of singlet and triplet excitons for efficient white organic light-emitting devices. *Nature* **2006**, *440* (7086), 908−12.
(29) Reineke, S.; Lindner, F.; Schwartz, G.; Seidler, N.; Walzer, K.; Lussem, B.; Leo, K. White organic light-emitting diodes with fluorescent tube efficiency. *Nature* **2009**, *459* (7244), 234−8.
(30) Wang, Q.; Ding, J.; Ma, D.; Cheng, Y.; Wang, L.; Jing, X.; Wang, F. Harvesting Excitons Via Two Parallel Channels for Efficient White Organic LEDs with Nearly 100% Internal Quantum Efficiency: Fabrication and Emission-Mechanism Analysis. *Adv. Funct. Mater.* **2009**, *19* (1), 84−95.
(31) Wang, Q.; Ding, J.; Ma, D.; Cheng, Y.; Wang, L.; Wang, F. Manipulating Charges and Excitons within a Single-Host System to Accomplish Efficiency/CRI/Color-Stability Trade-off for High-Performance OWLEDs. *Adv. Mater.* **2009**, *21* (23), 2397−2401.
(32) Sun, N.; Wang, Q.; Zhao, Y.; Chen, Y.; Yang, D.; Zhao, F.; Chen, J.; Ma, D. High-performance hybrid white organic light-emitting devices without interlayer between fluorescent and phosphorescent emissive regions. *Adv. Mater.* **2014**, *26* (10), 1617−1621.
(33) Wu, Z.; Luo, J.; Sun, N.; Zhu, L.; Sun, H.; Yu, L.; Yang, D.; Qiao, X.; Chen, J.; Yang, C.; Ma, D. High-Performance Hybrid White Organic Light-Emitting Diodes with Superior Efficiency/Color Rendering Index/Color Stability and Low Efficiency Roll-Off Based on a Blue Thermally Activated Delayed Fluorescent Emitter. *Adv. Funct. Mater.* **2016**, *26* (19), 3306−3313.
(34) Wu, Z.; Yu, L.; Zhou, X.; Guo, Q.; Luo, J.; Qiao, X.; Yang, D.; Chen, J.; Yang, C.; Ma, D. Management of Singlet and Triplet Excitons: A Universal Approach to High-Efficiency All Fluorescent WOLEDs with Reduced Efficiency Roll-Off Using a Conventional Fluorescent Emitter. *Adv. Opt. Mater.* **2016**, *4* (7), 1067−1074.
(35) Mayr, C.; Lee, S. Y.; Schmidt, T. D.; Yasuda, T.; Adachi, C.; Brütting, W. Efficiency Enhancement of Organic Light-Emitting Diodes Incorporating a Highly Oriented Thermally Activated Delayed Fluorescence Emitter. *Adv. Funct. Mater.* **2014**, *24* (33), 5232−5239.

DOI: 10.1021/acsphotonics.8b01724
ACS Photonics 2019, 6, 767−778